Coupled Energetics of λ *cro* Repressor Self-Assembly and Site-Specific DNA Operator Binding I: Analysis of *cro* Dimerization from Nanomolar to Micromolar Concentrations†

Paul J. Darling,‡ Jo M. Holt, and Gary K. Ackers*

Department of Biochemistry and Molecular Biophysics, Washington University School of Medicine, 660 South Euclid Avenue, St. Louis, Missouri 63110

Received April 25, 2000

ABSTRACT: The *cro* repressor from bacteriophage λ is an important and classical transcription regulatory protein that binds DNA operator sites as a dimer. Therefore, a complete understanding of gene regulation by *cro* requires knowledge of the coupled energetics of its protein dimerization and site-specific DNA binding. A method is described by which *cro* repressor can be labeled in vivo with [^{35}S]methionine to a specific activity of 2×10^{15} cpm/mol. As a prelude to binding studies, the association equilibrium of *cro* was determined over the range $10^{-9}-10^{-3}$ M using large-zone analytical gel chromatography with radiolabeled repressor. The data are best described by a monomer−dimer stoichiometry with an equilibrium constant of 3.07 (±1.08) $\times 10^6$ M^{-1} total *cro* monomer. Stokes radii for monomers and dimers were evaluated from the resolved gel partition coefficients. Under the conditions employed in this study (10 mM Bis-Tris, 200 mM KCl, 2.5 mM $MgCl_2$, 1 mM $CaCl_2$, 100 μg/mL BSA, pH 7.0, 20 °C), self-association of *cro* to species with assembly states greater than dimers is not observed.

The control of transcriptional initiation is brought about by a diverse array of protein−protein and protein−DNA interactions in equilibrium. For example, sequence-specific DNA binding by a transcriptional regulatory protein is often energetically coupled to the formation of a high-affinity association complex (cf. *1*). These observations necessitate that the linkage between protein assembly and DNA binding be understood explicitly in order to develop a mechanistic understanding of a given system of interest. Detailed understanding of how the physical−chemical principles are utilized then allows formulation of conceptual, predictive, in vivo models (*2, 3*). The inclusion of experimentally determined biophysical parameters is important for validation and testing such descriptive models. As a result, the roles of protein interactions, which mediate assembly and cooperativity, can be evaluated.

In bacteriophage λ, the delicate balance between two alternate life cycles, lysogeny and lysis, is controlled by *c*I and *cro* (*4*) as they self-assemble and bind to the six sites on the right and left operators (O_R and O_L) of the phage genome (*5, 6*). The dimerization and operator DNA binding reactions of *c*I have been well characterized (*7*−*10*). To build a more accurate understanding of gene control by the complex interplay between these two repressors, however, it is necessary to obtain more precise evaluation of the functional energetics of *cro* in its role as a transcriptional regulator. Interactions involving *cro* repressor and the right operator are diagrammed in Figure 1. Monomers are in dynamic equilibrium with dimers, which are the binding species (*5, 11, 12*). While dimers bind to the individual operator sites with an intrinsic free energy, they also exhibit an additional free energy of positive cooperativity when bound to adjacent operator sites. A complete characterization of *cro* binding to the right operator requires seven energetic terms: one for dimerization; three for intrinsic interaction between *cro* and the individual operator sites; and three for cooperative interaction. Since *cro* dimerization and operator binding are energetically coupled, the free energy contribution of the linked assembly reaction must ultimately be considered to correctly interpret the DNA binding data.

In the work presented here, *cro* self-assembly was addressed using gel permeation techniques. Chromatography allows detection of the eluting protein by several different methods including absorbance, fluorescence, and scintillation counting of radiolabeled repressor (*7, 13*). These methods allow the assembly of *cro* to be analyzed over a total protein concentration of $10^{-9}-10^{-2}$ M (*9*). Once information regarding the self-assembly of cro has been obtained, the concentration of the binding species can be explicitly calculated—a necessary step when considering DNA binding processes with linked assembly reactions.

MATERIALS AND METHODS

Chemicals and Biochemical Materials. Ampicillin, ammonium sulfate, bovine serum albumin (BSA, fraction V, protease free), guanidine hydrochloride (ultrapure), isopropyl β-D-thiogalactoside (IPTG), lysozyme, leupeptin, pepstatin A, phenylmethanesulfonyl fluoride (PMSF), poly(ethylenimine), and sodium deoxycholate were obtained from Sigma

† This work was supported by National Institutes of Health Grants GM-39343 and R37GM24486 and by Fellowship T32GM08492.

* To whom correspondence should be addressed. Phone: 314-362-0260, Fax: 314-747-3467, e-mail: ackers@biochem.wustl.edu.

‡ Current address: Department of Biochemistry and Biophysics, University of Pennsylvania School of Medicine, Philadelphia, PA.

10.1021/bi000935s CCC: $19.00
Published on Web 08/18/2000

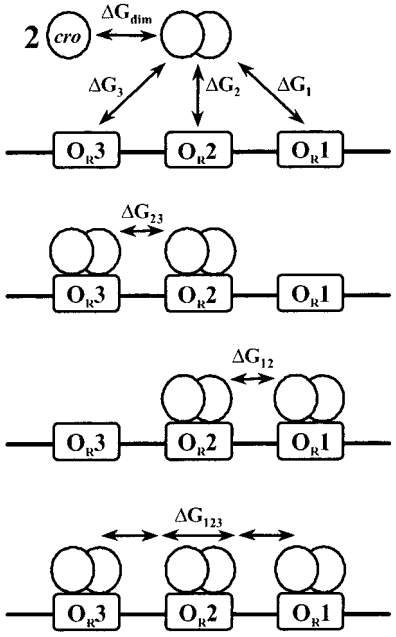

FIGURE 1: Interactions involving *cro* repressor and the right operator (O_R). O_R contains three 17 base pair binding sites, O_R1, O_R2, and O_R3, separated by spacers of 6 and 7 base pairs, respectively. *cro* repressor monomers consists of 66 amino acids. *cro* dimerizes (ΔG_{dim}) and binds the three O_R sites with intrinsic free energies ΔG_1, ΔG_2, and ΔG_3, corresponding to binding at sites O_R1, O_R2, and O_R3, respectively. Adjacently bound *cro* repressors exhibit a nonadditivity or cooperative free energy (ΔG_{12}, ΔG_{23}, ΔG_{123}).

Chemical Co. Electrophoresis grade acrylamide, ammonium persulfate, bis(acrylamide), and TEMED were from Bio-Rad. Acrylamide and bis(acrylamide) were deionized using Bio-Rad AG501-X8 mixed-bed resin prior to use. Bio-Gel P polyacrylamide gels were also from Bio-Rad.

L-[^{35}S]Methionine (in vivo cell label grade, 1000 Ci/mmol) was from Amersham. P-11 cellulose phosphate was from Whatman. Double-stranded native DNA cellulose (DS-DNA cellulose) and Hydroxyapatitie-Ultrogel (HAP-Ultrogel) were from Pharmacia Biotech.

Molecular size standards, used in calibrating the column and in determining Stokes radii, obtained from Sigma were the following: blue dextran, bovine pancreatic trypsin inhibitor (BPTI), cytochrome *c* (from horse heart), α-lactalbumin (type I from bovine milk), myoglobin (from horse heart), and L-tryptophan. RNase A, used in column calibration, as above, was from Pharmacia Biotech.

Protein Purification. The methods used to overexpress and purify *cro* from *E. coli* were adapted from (*14*). *cro* was overexpressed from the tac promoter on plasmid pAP119 (*15*) and purified from *Escherichia coli* strain X9T as described by Takeda et al. (*16*) with the modifications below.

E. coli strain X9T transformed with plasmid pAP119 was stored at −70 °C in Luria−Bertani (LB) medium with 30% glycerol. One hundred liters of LB/ampicillin (100 μg/mL) was inoculated and grown to an OD_{590} of ∼1.5. The culture was induced for 3 h with IPTG (100 μg/mL) and then reduced to 6 L by filtration. The cells were centrifuged at 7000*g* for 10−15 min and resuspended in 3 times their weight of lysis buffer [50 mM Tris-HCl (pH 8.0 at 4 °C), 10% sucrose (w/v), 10 mM EDTA, 50 mM KCl]. The slurry was flash-frozen in liquid nitrogen and stored at −70 °C in aliquots corresponding to 50 g of wet packed cells (WPC) per bottle (200 mL total).

All purification steps were performed at 4 °C or on ice. One hundred grams of WPC was thawed with shaking under a flow of warm water with constant agitation. The cell slurry remained below 4 °C during the thawing process. Protease inhibitors were added to a final concentration of 100 μg/mL (PMSF) and 1 μg/mL (pepstatin A and leupeptin). Cells were lysed using a Branson Sonifier model 250 with a half-inch probe. The slurry was sonicated for 15 s with a 90% pulse and then for 4 min and 45 s with a 10% pulse and allowed to chill on ice for 5 min between these 5 min pulse sequences. The pulse sequence was repeated 5 times. Additional PMSF was added after the third and fifth pulse sequences. KCl was added to a final concentration of 750 mM from a stock of 3 M in lysis buffer. The lysis slurry was centrifuged at 15000*g* for 40 min.

The supernatant was made 0.6% in PEI by addition from a 10% stock with constant, slow stirring (*17*) and centrifuged at 27500*g* for 50 min. Ammonium sulfate was added to 55% saturation (32.6 g/100 mL), and the precipitate was pelleted at 27500*g* for 50 min. The pellet was dissolved in (300 g/1200 mL) buffer C-100 [10 mM potassium phosphate (pH 8.0), 0.1 mM EDTA, 5% glycerol (v/v), 100 mM NaCl], and protease inhibitors were added as above. The resultant solution was dialyzed extensively against three changes of 4 L each of buffer C-100.

The pH and conductivity of the dialyzed sample were adjusted, if necessary, to match those of buffer C-100. The sample was loaded onto a Whatman P-11 cellulose phosphate column (400 mL, 5 × 20 cm, prepared according to package instructions and equilibrated using 3 column volumes of buffer C-100) at a linear flow rate of 0.26 cm/min. The column was washed with 1 volume of C-100. *cro* repressor was eluted using a 2 L linear gradient of buffer C from 100 to 600 mM NaCl. *cro* was found to elute at 450−550 mM NaCl. The corresponding fractions were pooled and concentrated to 40% of the original volume using an Amicon Filter/Concentrator equipped with a YM3 membrane. Protease inhibitors were added as above, and the resultant, concentrated pool of fractions was dialyzed extensively against three 1 L changes of buffer A-100 [10 mM potassium phosphate (pH 6.4), 5% glycerol (v/v), 100 mM KCl].

The dialyzed sample was clarified by centrifugation at 20000*g* for 20 min in a Sorvall SS-34 rotor. The collected precipitate contained some *cro* and a significant number of impurities. This step resulted in a significant enrichment of *cro* despite minor losses in yield. The dialyzed and clarified supernatant was loaded onto a Pharmacia HAP Ultrogel column (200 mL, 2.5 × 41 cm, preequilibrated in buffer A-100) at a linear flow rate of 0.41 cm/min. *cro* was eluted using a 1 L linear gradient of buffer A ranging from 100 to 500 mM KCl. *cro* elutes as a single peak with its maximum occurring at approximately 300 mM KCl. The relevant fractions were pooled, concentrated to 15−20% of the original volume, and dialyzed extensively against *cro* storage buffer [10 mM Tris-HCl (pH 7.4 at 4 °C), 0.1 mM EDTA, 200 mM KCl, 50% glycerol]. The purified repressor was determined to be greater than 95% pure as judged by Coomassie Brilliant Blue and silver staining of samples run on 15% SDS−polyacrylamide gels and stored at −20 °C.

Molar Absorbance Determination. The molar absorptivity of *cro* was determined according to the method of Gill and

von Hippel (*18*). The absorbance of repressor in standard buffer (10 mM Bis-Tris, 200 mM KCl, 2.5 mM $MgCl_2$, 1 mM $CaCl_2$, pH 7.0, 20 °C) was compared to the absorbance in standard buffer containing 6 M guanidine hydrochloride over a range of 10−500 μM total *cro* repressor. Samples were scanned from 200 to 350 nm on a Cary3 spectrophotometer with an averaging time of 0.1 s, a data interval of 0.5 nm, and a scan rate of 300 nm/min. The band-pass was 1 nm. Values of 4198 ± 14 M^{-1} cm^{-1} (0.571 ± 0.002 $mL \cdot mg^{-1} \cdot cm^{-1}$) at 278 nm and 77 467 ± 258 M^{-1} cm^{-1} (10.53 ± 0.04 $mL \cdot mg^{-1} \cdot cm^{-1}$) at 220 nm were determined from linear regression of triplicate experiments using a molecular weight of 7358 as determined from amino acid composition.

Purification of ^{35}S-Radiolabeled λ Phage cro Repressor. *cro* was overexpressed from the *tac* promoter on plasmid pAP119 (*15*) and purified from *Escherichia coli* strain RB791 [W3110 *lac*I^QL8] (*19*) as described above with minor modifications. The ^{35}S label was incorporated according to Beckett et al. (*7*) with the modifications below. Liquid scintillation counting was performed by mixing serial dilutions of labeled repressor of 0.5 mL total volume into 4 mL of liquid scintillation cocktail. Triplicate samples showed that 2.3×10^{15} cpm of ^{35}S label had been incorporated per mole of *cro* repressor. This corresponds to 1000 Ci/mol assuming a liquid scintillation counting efficiency for ^{35}S of 95% and 2.2 dpm/μCi.

Escherichia coli strain RB791 transformed with plasmid pAP119 was stored at −70 °C in Luria−Bertani (LB) medium with 30% glycerol. Bacteria were grown in 50 mL of Modified Minimal Media [M9 salts (pH 7.4), 1% (w/v) glucose, 0.14 mM Na_2SO_4, 2 mM $MgCl_2$, 0.1 mM $CaCl_2$] (*19*) with 100 μg/mL ampicillin in a sterile 250 mL Erlenmeyer flask. At an OD_{590} of 0.7−0.9, 10 mL of the 50 mL culture was aliquoted to a second, sterile, prewarmed 250 mL Erlenmeyer flask. The 10 mL culture was induced for 5 min with IPTG (100 μg/mL). [^{35}S]Methionine (10 mCi/mL, 1000 Ci/mmol) was added to final concentration of 1 μM methionine, corresponding to 1 mCi of label/mL of culture. The culture was grown for an additional hour.

The cells were harvested by centrifugation, resuspended in 50 μL of lysis buffer, and transferred to a sterile eppendorf tube. Protease inhibitors were added as described in the purification scheme for unlabeled *cro* repressor, and the cell slurry was stored at −70 °C overnight.

Cells were thawed on ice and lysed by addition of lysozyme to a final concentration of 600 μg/mL from a stock of 30 mg/mL made fresh in lysis buffer. Lysis was then continued on ice for 1 h. To increase lysis efficiency, sodium deoxycholate was added to a final concentration of 0.05% from a stock solution made fresh in water and NaOH (6.1 mL of H_2O, 0.15 mL of 5 M NaOH, 0.25 g of sodium deoxycholate) (*20*). Lysis was continued for an additional hour on ice.

$MgCl_2$ (20 mM), $CaCl_2$ (1 mM), and DNase I (10 μg/mL) were added, and the solution was incubated on ice for 30−60 min. KCl (750 mM) was added from a 3 M stock in lysis buffer, and the cell debris was pelleted by centrifugation in a tabletop micro-centrifuge at 10 000 rpm for 2−5 min.

The supernatant from the lysis step was brought to 0.6% in PEI by dropwise addition from a 10% stock (*17*) and centrifuged at 10 000 rpm for 30 min in a tabletop micro-centrifuge, and the pellet was discarded. Ammonium sulfate was added to the supernatant to 55% saturation (0.326 g/mL), and the precipitate was pelleted by centrifugation at 10 000 rpm for 30 min in a tabletop micro-centrifuge. The pellet was dissolved in 750 μL of buffer C-100 and dialyzed extensively against buffer C-100.

The sample was loaded onto a Whatman P-11 cellulose phosphate column (1.5 mL, 0.5 × 7.6 cm, prepared according to package instructions and equilibrated using 3 column volumes of buffer C-100) at a linear flow rate of 0.41 cm/min. The column was washed with 2 volumes of buffer C-100 and 2 volumes of buffer C-200. A step gradient consisting of 1 volume each of buffer C containing 200, 300, 400, and 500 mM NaCl, and 5 volumes of buffer C-600 was used. *cro* eluted from 450 to 550 mM NaCl as determined by SDS−polyacrylamide gel analysis of the collected fractions (*21*). Relevant fractions were pooled and dialyzed extensively against buffer D-50 [50 mM Tris-HCl (pH 7.4 at 4 °C), 5 mM EDTA, 5% glycerol, 50 mM NaCl].

The dialyzed sample was loaded onto a Pharmacia Double Stranded Native DNA−cellulose column (0.75 mL, 0.5 × 3.8 cm, equilibrated in buffer D containing 1500 mM NaCl and washed with 3 volumes of buffer D-50) at a linear flow rate of 0.41 cm/min. The column was washed with 2 volumes of buffer D-50, 8 volumes of buffer D-100, and then 5 volumes of buffer D-150. Radiolabeled *cro* repressor was eluted with 6 volumes of buffer D-400. Fractions were analyzed by SDS−polyacrylamide gel electrophoresis, and the relevant fractions were pooled and concentrated on a Centricon 3 for 2−3 h. The concentrated sample was dialyzed extensively against *cro* storage buffer. Sample concentration was determined by absorbance measurements at 278 nm of serial dilutions from the stock solution and by subsequent linear regression. The repressor was determined to be greater than 95% pure as judged by silver staining and autoradiography of samples run on 15% SDS−polyacrylamide gels.

Analytical Gel Chromatography. BioRad BioGel P-30 columns (1 × 45 cm, 35 mL total volume) were constructed as described in Valdes and Ackers (*22*) and poured according to Turner (*23*). The column was equilibrated and maintained in Standard Buffer (10 mM Bis-Tris, 200 mM KCl, 2.5 mM $MgCl_2$, 1 mM $CaCl_2$, pH 7.0, 20 °C) plus 0.01% sodium azide (SB +azide). Unless otherwise noted, all tubing was Tygon with an inner diameter of 1/32 in. and an outer diameter of 3/32 in. The flow rate was regulated using a Rainin Rabbit II Peristaltic Pump fitted with silicon rubber tubing (Rainin) to brake the native flow rate to 14.3−14.7 mL/h. Flow rates were determined by the weight average of every tenth fraction of collected column eluant and found to vary ±0.005 mL/fraction (±2%). Before each experiment, the azide was washed out and the column was equilibrated in SB plus 100 μg/mL BSA (SB+BSA).

Large-zone (25−30 mL) experiments were carried out as described in Beckett et al. (*7*). High concentration zones were prepared by weight dilution of stock, unlabeled *cro* solutions into SB+BSA followed by the addition of very low concentration (10^{-9} M) of radiolabeled *cro*. Low concentration zones were prepared by volume dilution of stock radiolabeled repressor into SB+BSA. Plateau radioactivity levels of the large-zone eluates ranged from 4000 to 40 000 cpm/mL.

Samples were monitored at 278 or 220 nm using a Shimadzu 150 dual beam spectrophotometer connected to a Linear brand strip chart recorder. The effluent tubing from the spectrophotometer was connected to an Isco Retriever II fraction collector. Fractions were collected in five-drop (~0.25 mL) increments into preweighed plastic scintillation vials and mixed with 4.0 mL of Aquasol 2 (Dupont) scintillation fluid for counting. Elution profiles were determined optically or by scintillation counting of collected fractions. Sample counting was performed for 2 min on an LKB (Wallace) 1208 Rackbeta Liquid Scintillation Counter.

Analysis of Chromatographic Data. Data were plotted as plateau concentration versus volume. Zones with concentrations greater than 6 μM total *cro* required an additional correction to account for volume changes in the collected fractions due to decreased drop size. This decreased fraction volume resulted from surface tension variations (*24*) and correlated with large-zone elution. The flow rate was corrected by applying a linear transition between the average fraction volume of the baseline (V_1) and the fraction volume of the plateau (V_2). The total eluted volume was calculated as follows:

$$\text{total eluted volume} = \sum_{i=1}^{A} V_i + \sum_{j=A+1}^{B} V_j + \sum_{k=B+1}^{C} V_k + \sum_{l=C+1}^{D} V_l + \sum_{m=D+1}^{E} V_m \quad (1)$$

where *i, j, k, l,* and *m* are fraction numbers, *A* is the last fraction number before elution of the large zone, *B* is the last fraction number in the leading edge (before plateau), *C* is the last fraction number in the plateau region (before beginning of trailing edge), *D* is the last fraction number in the trailing edge (before return to baseline), *E* is the last collected fraction number, and

$$V_i = V_1 \text{ when } i \le A \quad (2)$$

$$V_j = V_1 - \left(\left[\frac{j-A}{B-A}\right] \cdot \left|V_1 - V_2\right|\right) \quad (3)$$

$$V_k = V_2 \text{ when } B < k \le C \quad (4)$$

$$V_l = \left(\left[\frac{l-C}{D-C}\right] \cdot \left|V_1 - V_2\right|\right) + V_2 \quad (5)$$

$$V_m = V_1 \text{ when } m > D \quad (6)$$

The elution profiles were corrected before centroid volume determination. Elution volumes (V_e) were determined as the equivalent sharp boundaries (centroids) of the leading edges of the zone by numerical integration [Figure 2; see also (*22*)]. The elution of a macromolecule is represented by the partition coefficient (*25*) which is the fraction of the solvent volume within the gel matrix that is accessible to the macromolecule. Weight average partition coefficients ($\bar{\sigma}_w$) were calculated relative to totally excluded and included standards by

$$\bar{\sigma}_w = (V_e - V_o)/V_i \quad (7)$$

where V_o and V_i are the void and internal volumes of the column, with values of 10.75 ± 0.05 and 24.23 ± 0.07 mL, respectively, and were determined by small-zone analysis

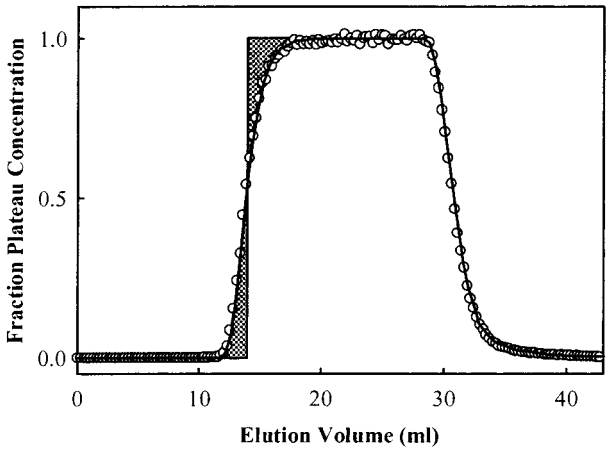

FIGURE 2: Radiolabeled repressor represents the bulk properties of *cro* solutions. The plateau concentration for both profiles is 10^{-5} M total *cro* monomer. The circles represent an elution profile that was monitored by scintillation counting of collected fractions. The solid line represents a profile that was monitored spectroscopically. The vertical line is the centroid volume, V_e, representing the center of mass of the leading edge (*22*). The identical centroid volumes demonstrate that radiolabeled repressor represents the bulk properties of the entire solution.

of Blue Dextran (5 mg/mL in SB+azide) and L-tryptophan (0.3 mg/mL in SB+azide) (*22*, *26*). The resulting data, $\bar{\sigma}_w$ versus [cro total], were fit to a monomer−dimer stoichiometric model using nonlinear least squares regression (*27*), on the following equations:

$$\bar{\sigma}_w = f_1\sigma_m + (1 - f_1)\sigma_d \quad (8)$$

$$f_1 = [-1 + (1 + 8K_{dim}C_T)^{1/2}]/4K_{dim}C_T \quad (9)$$

where σ_m and σ_d are partition coefficients of monomers and dimers, respectively, f_1 is the fraction of monomer, C_T is the total protein concentration, and K_{dim} is the resolved equilibrium association constant.

Partition coefficients were determined for molecular size standards and were transformed as the inverse error function complement ($erfc^{-1}\sigma_j$) to yield a linear relationship with the molecular Stokes radius (*r*) (*28*):

$$r_j = a_0 + b_0(erfc^{-1}\sigma_j) \quad (10)$$

where a_0 and b_0 are the calibration constants for a given column. Hydrated radii corresponding to monomer and dimer endpoints were calculated from calibration curves using the molecular size standards cytochrome *c* (16.4 Å), α-lactalbumin (19.4 Å), myoglobin (20.7 Å) (*29*), BPTI (17.0 Å), lysozyme (19.4 Å) (*30*), and RNase A (16.3 Å) (*31*).

Data were analyzed to determine the best-fit model-dependent parameters, which yielded the minimum variance. Joint confidence intervals for the fitted parameters were estimated according to the method of Box (*32*). Confidence intervals (67%) correspond to approximately one standard deviation.

RESULTS

Protein Purification and Molar Absorbance Determination. The purification protocol presented here yielded 200−300 mg of *cro* from 100 g of WPC. The purified protein was >95% pure as judged by silver staining of samples

electrophoresed on 15% SDS−polyacrylamide gels and had 100% DNA binding activity as determined by stoichiometric binding assays [see (*33*)].

The molar absorbance of *cro* determined in this study was 4198 ± 14 M^{-1} cm^{-1} (0.571 ± 0.002 mL·mg^{-1}·cm^{-1}) at 278 nm and 77 467 ± 258 M^{-1} cm^{-1} (10.53 ± 0.04 mL·mg^{-1}·cm^{-1}) at 220 nm. These values differ only slightly from the summed molar absorbancies of the contributing amino acids (three tyrosines per monomer) over a wide concentration range (10^{-7}−10^{-3} M), suggesting minimal changes in hypo- or hyperchromicity due to intra- or intermolecular interactions (*18, 34*).

^{35}S Protein Labeling and Purification. The procedures used for bacterial growth and in vivo labeling were adapted from Beckett et al. (*7*) to maximize the specific activity and quantity of the *cro* repressor preparation. The specific activity of the purified *cro* repressor was 2 × 10^{15} cpm/mol (1000 Ci/mol), which is high enough to detect the protein at a concentration as low as 10^{-9} M. The small quantity of cells and high concentration of radioactivity used during in vivo labeling required replacement of the usual sonication step with a detergent−lysozyme lysis step. The relatively high concentration of added lysozyme required a double-stranded native DNA−cellulose column chromatography step to separate the lysozyme from *cro* repressor as both proteins display similar isoelectric points (pI ≥ 10), preventing separation by ion exchange methods. Silver staining revealed the presence of unlabeled proteins while autoradiography allowed visualization of labeled proteins, present in low concentrations but with very high specific activity. This cross-check was necessary for accurate concentration determination of the radiolabeled repressor and to ensure that the radioactivity associated with eluting zones during gel chromatography represented pure *cro* repressor.

Dimerization Energetics. Elution profiles for two chromatographic zones of *cro* repressor are shown in Figure 2. The profiles exhibited boundary sharpening on the leading edge of the solute zone and a corresponding boundary spreading on the trailing side which are characteristic of self-associating solutes on sieving columns (*13*). The vertical line represents the centroid volume, V_e, and denotes the center of mass of the leading edge. Identical centroid volumes from the two profiles, measured by absorbance and by radioactivity, demonstrate that the added radiolabeled repressor is representative of the sample's bulk solution properties.

The centroid of the leading edges of elution profiles decreased with increasing *cro* concentrations over the range from nanomolar to millimolar total *cro* repressor (Figure 3). This shift in the centroid volume with increasing concentration reflects an increase in average molecular size as the fraction of dimers increases according to mass action. The difference in elution volume between the monomeric and dimeric species was ~3 mL.

Weight average partition coefficients as a function of monomer concentration are shown in Figure 4. The solid curve depicts the best fit to a monomer−dimer stoichiometric model of assembly (eqs 8 and 9). The data spanned 5 orders of magnitude in protein concentration and were well described by the assembly model employed. The use of an assembly model that limits the stoichiometry to 2 was supported by the fact that column calibration as a function of apparent molecular weight suggested that assemblies of

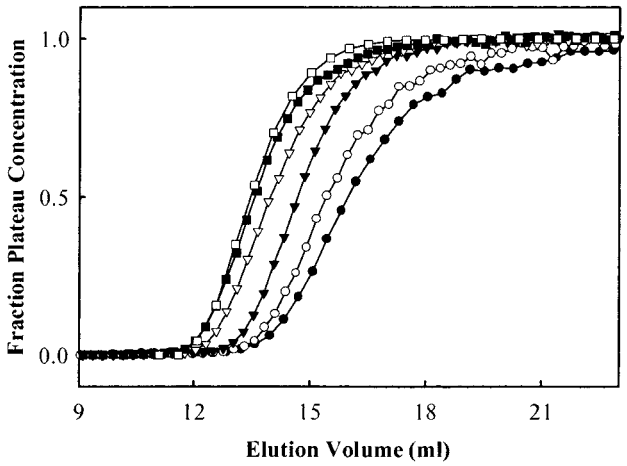

FIGURE 3: Concentration dependence of the centroid volume reveals protein self-association. Shown are the leading boundaries of six large zones of *cro* repressor at plateau concentrations: 3 × 10^{-9} (●), 1 × 10^{-7} (○), 3 × 10^{-7} (▼), 3 × 10^{-6} (▽), 3 × 10^{-5} (■), 4 × 10^{-4} (□) M total *cro* monomer. Boundary positions shift toward lower elution volumes with increasing *cro* concentration, reflecting the increase in average molecular size as the fraction of dimers increases according to mass action.

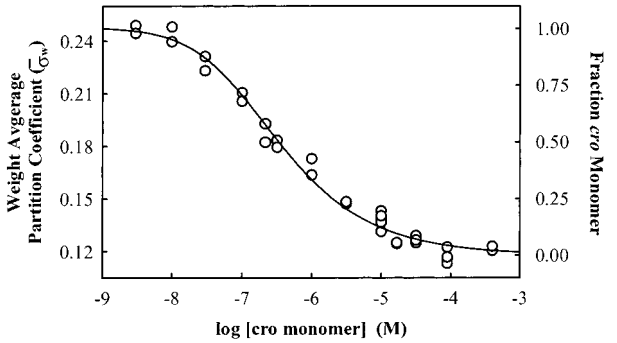

FIGURE 4: Dimer association curve for *cro* repressor: Weight average partition coefficients ($\bar{\sigma}_w$) obtained as a function of total *cro* monomer concentration. Weight average partition coefficients can be expressed as a function of fraction monomer (f_1), monomer partition coefficient (σ_m), and dimer partition coefficient (σ_d) according to eq 8. Fraction monomer values as a function of total *cro* monomer concentration are shown on the right ordinate. The solid line represents a best fit of the data to a monomer−dimer stoichiometric model.

three or more *cro* monomers would exhibit a partition coefficient of 0.03 at the high concentration endpoint while values of 0.12 are observed. Dimerization studies of λ *c*I repressor showed a sharp drop in $\bar{\sigma}_w$ at high protein concentrations (1−10 μM), suggesting assembly to higher order species (*7, 35*). This observation was confirmed by sedimentation equilibrium studies (*36*). In the work presented here, the high concentration endpoint corresponded to a stable dimer species and was well-defined by the data suggesting that any assembly to higher order species must occur outside the concentration range used in this study.

The buffer used in this work contained 100 μg/mL BSA. This component was included to block nonspecific adsorption of *cro* to the column matrix at low concentrations (<3 × 10^{-7} M). This slight sticking was detected by asymmetry in the elution profiles of zones at low concentrations and by incomplete recovery of the loaded protein. Experiments conducted at plateau concentrations of 10^{-5} M in the presence and absence of BSA showed equivalent centroid volumes

Table 1: Resolved Parameters for *cro* Monomer−Dimer Equilibrium

K_{eq}[a]		3.07 (±1.08) × 10^6 M^{-1}
ΔG_{dim}[b]		−8.7 ± 0.2 kcal·mol^{-1}
Stokes radius	monomer	14.6 ± 0.2 Å
	dimer	17.0 ± 0.2 Å
R_S/r_0[c]	monomer	1.14 ± 0.02 Å
	dimer	1.04 ± 0.01 Å
hydration (w_{max})[d]	monomer	0.33 ± 0.04 g of H_2O/g of *cro*
	dimer	0.10 ± 0.02 g of H_2O/g of *cro*
(variance of fit)$^{1/2}$		0.005

[a] Association constant. [b] Standard Gibbs free energy of dimerization with 67% confidence intervals. [c] Ratio of Stokes radius to calculated anhydrous molecular radius. [d] Maximal hydration (grams of water per gram of protein).

(data not shown) indicating that the added BSA had no effect on the assembly properties of *cro* (*7*).

Molecular Size and Shape Parameters. Partition coefficients determined for the monomer and dimer species were used in conjunction with column calibration data to calculate Stokes radii for *cro* monomers and dimers; values are shown in Table 1. The precision in R_S reported in Table 1 reflects 67% confidence intervals of the fitted partition coefficients. The inherent precision of molecular radius determinations of globular proteins by gel partitioning methods has been explored in detail and shown to be ±0.2 Å (*26*).

The transport behavior of a molecule provides information about its shape and hydration. The translational frictional coefficient, *f*, is thus related to fluid viscosity by Stokes' law (for a sphere):

$$f = 6\pi\eta R_S \tag{11}$$

where η is the viscosity of water at 20 °C and R_S is the Stokes' radius of the molecule. The frictional coefficient of an ideal unsolvated spherical molecule with the same mass and partial specific volume as the protein under consideration is described by

$$f_0 = 6\pi\eta r_0 \tag{12}$$

where r_0 is the molecular radius of the spherical anhydrous protein and can be calculated ab initio by equating the anhydrous molecular volume ($M\bar{V}/N$) to a sphere of radius r_0:

$$\frac{M\bar{V}}{N} = \frac{4}{3}\pi r_0^3 \tag{13}$$

After rearrangement:

$$r_0 = \left(\frac{3M\bar{V}}{4\pi N}\right)^{1/3} \tag{14}$$

where M is the molecular weight of the protein, $\bar{V}$ is the partial specific volume, and N is Avogadro's number. Deviations of the ratio of f/f_0 from unity reflect nonspherical molecular shape and/or hydration effects. A value for r_0^{mon} of 12.9 Å was calculated using M = 7358 and $\bar{V}$ = 0.740 cm^3/g (calculated from amino acid composition) (*37*) for the anhydrous radius of *cro* monomer. An apparent Stokes radius (R_S^{mon}) of 14.6 Å was determined experimentally, giving an $(R_S/r_0)_{mon}$ value of 1.14. Similarly, for *cro* dimers, r_0^{dim} = 16.3 Å and R_S^{dim} = 17.0; thus, $(R_S/r_0)_{dim}$ = 1.04. *cro* thus was found to exhibit a shift toward compaction upon dimerization, reflecting plasticity of the repressor that has been shown to be necessary for operator binding (*38*−*40*). This compaction may be due in part to the insertion of phenylalanine 58 of one monomer into the core of its partner monomer upon dimerization (*41*): the burial of such a protruding residue may decrease the apparent frictional coefficient of the dimer relative to that for a "doubled monomer."

The frictional coefficient contains information about molecular shape and hydration effects. Accordingly, an upper limit on the contributions of hydration can be calculated by assuming that all deviations of f/f_0 from unity are due to hydration such that

$$\frac{f}{f_0} = \frac{R_S}{r_0} = \left(\frac{\bar{V}_{cro} + w_{max}\bar{V}_{H_2O}}{\bar{V}_{cro}}\right)^{1/3} \tag{15}$$

This equation can be rearranged to

$$w_{max} = \frac{\bar{V}_{cro}}{\bar{V}_{H_2O}}\left[\left(\frac{R_S}{r_0}\right)^3 - 1\right] \tag{16}$$

where w_{max} is the maximal hydration in grams of H_2O bound per gram of *cro*, $\bar{V}_{cro}$ is the partial specific volume of *cro* calculated from amino acid composition, and $\bar{V}_{H_2O}$ is the partial specific volume of bound water. For a spherical molecule with $(R_S/r_0)_{mon}$ = 1.14, w_{max} is 0.33 g of H_2O per gram of *cro* monomer; dimers have a value of $(R_S/r_0)_{dim}$ = 1.04 which corresponds to a w_{max} of 0.17 g of H_2O per gram of *cro* dimer. Maximal values of hydration for both monomeric and dimeric *cro* species are similar to a "typical" value of 0.25 g of H_2O per gram of protein. A value of 0.357 g of H_2O per gram of *cro* was calculated for both monomers and dimers according to hydration values for individual amino acids (*42*). The value of hydration for the monomer determined experimentally agrees with the calculated value while that for the dimer is smaller by a factor of 2.

DISCUSSION

To generate a more complete model for gene regulation in bacteriophage λ, the roles of the interacting components have required extensive exploration. For *cro* repressor, an essential step to the understanding of its function as a transcriptional regulator is the investigation of its assembly to a high-affinity DNA binding species. In this work, high-precision analytical gel chromatography (AGC) was used to measure the monomer−dimer equilibrium assembly properties of the bacteriophage λ *cro* repressor. Previous studies involving DNA binding of *cro* have not incorporated the contribution of the linked dimerization to the overall binding process (*6*, *12*, *16*, *43*−*49*). The results presented here demonstrate a free energy change upon dimerization of −8.7 kcal/mol. This comparatively weak dimerization free energy precludes accurate interpretation of *cro*−O_R interactions with site-specific binding constants in the picomolar range (*33*). In addition, it challenges the traditional view that *cro* repressor exists as a dimer at all concentrations (*6*, *12*).

Use of ^{35}S-Labeled cro and Analytical Gel Chromatography. The use of protein labeled to a very high specific activity (2 × 10^{15} cpm/mol) has permitted an accurate

determination of the equilibrium association constant because the partition coefficient can be determined at total monomer concentrations as low as 1×10^{-9} M. Such low concentrations of *cro* have been inaccessible to spectroscopic analysis due to the protein's small extinction coefficient. In addition, the elution profile monitored by scintillation counting has a signal that is unaffected by the presence of 100 μg/mL BSA (used to block nonspecific adsorption to the column at low *cro* concentrations) while that of the profile that is optically monitored further demonstrates an increase in background noise. Use of a radiolabeled tracer allows circumvention of issues related to tight assembly constants, low optical signal, and the need to include additional components which block nonspecific adsorption.

The gel chromatography data presented in this study span 5 orders of magnitude in total repressor concentration. This broad concentration range defines the asymptotic regions of the assembly curve well and, consequently, allows accurate resolution of the endpoints. Sufficient data in these regions are necessary to assign the stoichiometric model of assembly. A model that limits the stoichiometry to 2 is supported by the partition coefficients measured at high protein concentrations (see Results). These observations eliminate the need to consider higher order assembly under the conditions and concentrations used in this study.

Molecular Shape and Size Parameters. The Stokes radii obtained in this study for *cro* monomers and dimers are within the range of values expected for molecules of corresponding molecular weights, suggesting that the frictional properties of *cro* are similar to those of other globular proteins under the conditions used in this study. The apparent Stokes radius of 17.0 Å determined for *cro* dimers is smaller than that determined for side-by-side association and supports the possibility that *cro* may undergo an induced fit to bind DNA. It has been found that, to accommodate the 34 Å center-to-center distance of the major groove on B-form DNA, *cro* dimers reposition the α3 recognition helices and widen the channel into which the DNA backbone fits (*38, 40*).

Summary. For years, *cro* was thought to assemble from monomers to dimers in the subnanomolar concentration range (*5, 6*). First efforts to address this issue involved small-zone gel chromatography and indicated that a monomer−dimer equilibrium may be occurring in the micromolar to submicromolar range (*44*). Additional investigations of the assembly properties of *cro* using sedimentation equilibrium and gel chromatography relied heavily on data from engineered *cro* mutants (*50*). These mutant-dependent results suggested a dissociation constant of wild-type *cro* dimers in the micromolar range. Studies with the *c*I repressor showed, however, that hydrodynamic properties, such as Stokes radii and assembly free energies, are significantly altered by single point mutations (*35*). The work presented here uses thermodynamically rigorous techniques (*51*) and does not rely on data from mutant repressors to draw any conclusions about the assembly reaction. Accordingly, this work is the first rigorous evaluation of the dimerization properties of the *cro* repressor.

This study provides the necessary prelude to exploration of the complex linkage between subunit assembly and DNA binding by the λ *cro* repressor. Extensions of the present work may include investigating the linkage of other thermodynamic driving forces such as temperature, pH, and salt to the assembly properties of *cro*. Comparing the solution dependence of *cro* dimerization with that of *c*I repressor will provide a framework for exploring the differential transcriptional regulatory roles of these two repressors within the context of their self-assembly. In addition, knowledge of the temperature dependence of *cro* dimerization may provide information on the thermodynamic "cost" for formation of the flexible "ball-and-socket joint" formed by burial of Phe58 of one monomer into the core of the other (*41*). A complete thermodynamic description of *cro* association may be expected to provide additional rules that are central to the understanding of the mechanisms by which transcriptional regulatory molecules function.

REFERENCES

1. Wong, I., and Lohman, T. M. (1995) *Methods Enzymol. 259*, 95−127.
2. Ackers, G. K., Johnson, A. D., and Shea, M. A. (1982) *Proc. Natl. Acad. Sci. U.S.A. 79*, 1129−1133.
3. Shea, M. A., and Ackers, G. K. (1985) *J. Mol. Biol. 181*, 211−230.
4. Herskowitz, I., and Hagen, D. (1980) *Annu. Rev. Genet. 14*, 399−445.
5. Johnson, A. D., Pabo, C. O., and Sauer, R. T. (1980) *Methods Enzymol. 65*, 839−856.
6. Ptashne, M. (1986) *A Genetic Switch, Gene Control and Phage Lambda*, Second ed., Cell Press, Cambridge, MA, and Blackwell, Palo Alto, CA.
7. Beckett, D., Koblan, K. S., and Ackers, G. K. (1991) *Anal. Biochem. 196*, 69−75.
8. Koblan, K. S., and Ackers, G. K. (1991) *Biochemistry 30*, 7822−7827.
9. Koblan, K. S., and Ackers, G. K. (1991) *Biochemistry 30*, 7817−7821.
10. Koblan, K. S., and Ackers, G. K. (1992) *Biochemistry 31*, 57−65.
11. Anderson, W. F., Ohlendorf, D. H., Takeda, Y., and Matthews, B. W. (1981) *Nature 290*, 754−758.
12. Johnson, A., Meyer, B. J., and Ptashne, M. (1978) *Proc. Natl. Acad. Sci. U.S.A. 75*, 1783−1787.
13. Ackers, G. K. (1970) *Adv. Protein Chem. 24*, 343−446.
14. Takeda, Y., Folkmanis, A., and Echols, H. (1977) *J. Biol. Chem. 252*, 6177−6183.
15. Pakula, A. A., Young, V. B., and Sauer, R. T. (1986) *Proc. Natl. Acad. Sci. U.S.A. 83*, 8829−8833.
16. Takeda, Y., Kim, J. G., Caday, C. G., Steers, E., Jr., Ohlendorf, D. H., Anderson, W. F., and Matthews, B. W. (1986) *J. Biol. Chem. 261*, 8608−8616.
17. Burgess, R. R. (1991) *Methods Enzymol. 208*, 3−10.
18. Gill, S., C., and von Hippel, P. H. (1989) *Anal. Biochem. 182*, 319−326.
19. Brent, R., and Ptashne, M. (1981) *Proc. Natl. Acad. Sci. U.S.A. 78*, 4204−4208.
20. Lohman, T. M., Green, J. M., and Beyer, R. S. (1986) *Biochemistry 25*, 21−25.
21. Laemmli, U. K. (1970) *Nature 227*, 680−685.
22. Valdes, R., Jr., and Ackers, G. K. (1979) *Methods Enzymol. 61*, 125−142.
23. Turner, G. J. Ph.D. Thesis (1989), *Department of Biology*, p 386, Johns Hopkins University, Baltimore, MD.
24. Scopes, R. K. (1994) *Protein Purification, Principles and Practice*, Third ed., Springer, New York.
25. Ackers, G. K. (1967) *J. Biol. Chem. 242*, 3026−3034.
26. Warshaw, H. S., and Ackers, G. K. (1971) *Anal. Biochem. 42*, 405−421.
27. Johnson, M. L., and Frasier, S. G. (1985) *Methods Enzymol. 117*, 301−342.
28. Ackers, G. K. (1967) *J. Biol. Chem. 242*, 3237−3238.
29. Andrews, P. (1970) *Methods Biochem. Anal. 18*, 1−53.
30. Squire, P. G., and Himmel, M. E. (1979) *Arch. Biochem. Biophys. 196*, 165−177.

31. Sorensen, B. R., and Shea, M. A. (1996) *Biophys. J.* 71, 3407−3420.
32. Box, G. D. P. (1960) *Ann. N.Y. Acad. Sci. 86*, 792.
33. Darling, P. J., Holt, J. M., and Ackers, G. K. (2000) *J. Mol. Biol.* (in press).
34. Van Holde, K. E. (1971) *Physical Biochemistry*, First ed., Prentice Hall, Inc., Englewood Cliffs, NJ.
35. Burz, D. S., Beckett, D., Benson, N., and Ackers, G. K. (1994) *Biochemistry 33*, 8399−8405.
36. Burz, D. S., and Ackers, G. K. (1996) *Biochemistry 35*, 3341−3350.
37. Durchschlag, H. (1986) in *Thermodynamic Data for Biochemistry and Biotechnology* (Hinz, H.-J., Ed.) pp 45−128, Springer-Verlag, Berlin.
38. Brennan, R. G., Roderick, S. L., Takeda, Y., and Matthews, B. W. (1990) *Proc. Natl. Acad. Sci. U.S.A. 87*, 8165−8169.
39. Matsuo, H., Shirakawa, M., and Kyogoku, Y. (1995) *J. Mol. Biol. 254*, 668−680.
40. Ohlendorf, D. H., Tronrud, D. E., and Matthews, B. W. (1998) *J. Mol. Biol. 280*, 129−136.
41. Albright, R. A., and Matthews, B. W. (1998) *J. Mol. Biol. 280*, 137−151.
42. Kuntz, I. D., Jr., and Kauzmann, W. (1974) *Adv. Protein Chem. 28*, 239−345.
43. Boschelli, F. (1982) *J. Mol. Biol. 162*, 267−282.
44. Boschelli, F., Arndt, K., Nick, H., Zhang, Q., Lu, P., and Takeda, Y. (1982) *J. Mol. Biol. 162*, 251−266.
45. Johnson, A. D., Meyer, B. J., and Ptashne, M. (1979) *Proc. Natl. Acad. Sci. U.S.A. 76*, 5061−5065.
46. Kim, J. G., Takeda, Y., Matthews, B. W., and Anderson, W. F. (1987) *J. Mol. Biol. 196*, 149−158.
47. Ptashne, M., Jeffrey, A., Johnson, A. D., Maurer, R., Meyer, B. J., Pabo, C. O., Roberts, T. M., and Sauer, R. T. (1980) *Cell 19*, 1−11.
48. Takeda, Y., Ross, P. D., and Mudd, C. P. (1992) *Proc. Natl. Acad. Sci. U.S.A. 89*, 8180−8184.
49. Takeda, Y., Sarai, A., and Rivera, V. M. (1989) *Proc. Natl. Acad. Sci. U.S.A. 86*, 439−443.
50. Jana, R., Hazbun, T. R., Mollah, A. K., and Mossing, M. C. (1997) *J. Mol. Biol. 273*, 402−416.
51. Ackers, G. K. (1975) in *The Proteins* (Neurath, H., and Hill, R., Eds.) pp 1−94, Academic Press, Inc., New York.

BI000935S